KeAi
CHINESE ROOTS
GLOBAL IMPACT

Available online at www.sciencedirect.com

ScienceDirect

Green Energy & Environment 6 (2021) 432–443

www.keaipublishing.com/gee

Research paper

Machine learning-based ionic liquids design and process simulation for CO_2 separation from flue gas

Kai Wang [a], Huijin Xu [b], Chen Yang [a,*], Ting Qiu [a,*]

[a] *Engineering Research Center of Reactive Distillation, Fujian Province Higher Education Institutes, College of Chemical Engineering, Fuzhou University, Fuzhou, Fujian, 350116, China*

[b] *China-UK Low Carbon College, Shanghai Jiao Tong University, Shanghai, 200240, China*

Received 30 August 2020; revised 19 December 2020; accepted 22 December 2020
Available online 24 December 2020

Abstract

Rational design of ionic liquids (ILs), which is highly dependent on the accuracy of the model used, has always been crucial for CO_2 separation from flue gas. In this study, a support vector machine (SVM) model which is a machine learning approach is established, so as to improve the prediction accuracy and range of IL melting points. Based on IL melting points data with 600 training data and 168 testing data, the estimated average absolute relative deviations (AARD) and squared correlation coefficients (R^2) are 3.11%, 0.8820 and 5.12%, 0.8542 for the training set and testing set of the SVM model, respectively. Then, through the melting points model and other rational design processes including conductor-like screening model for real solvents (COSMO-RS) calculation and physical property constraints, cyano-based ILs are obtained, in which tetracyanoborate $[TCB]^-$ is often ruled out due to incorrect estimation of melting points model in the literature. Subsequently, by means of process simulation using Aspen Plus, optimal IL are compared with excellent IL reported in the literature. Finally, 1-ethyl-3-methylimidazolium tricyanomethanide [EMIM][TCM] is selected as a most suitable solvent for CO_2 separation from flue gas, the process of which leads to 12.9% savings on total annualized cost compared to that of 1-ethyl-3-methylimidazolium bis(trifluoromethylsulfonyl)amide [EMIM][Tf_2N].

Keywords: Ionic liquid; Rational design; CO_2 separation; Support vector machine; Process simulation

1. Introduction

Currently, with the development of industry and the intensification of human activities, carbon dioxide, as one of the greenhouse gases, increases rapidly year by year. According to the "Greenhouse Gas Bulletin" released by the World Meteorological Organization [1], the global average carbon dioxide concentration reached 407.88 ppm in 2018, which is 147% of the pre-industrial level in 1750. It has triggered many natural disasters such as melting glaciers and climate change. The numerous emissions of CO_2 mainly come from the burning of fossil energy for generating electricity. Based on the "2018 Global Energy and Carbon Dioxide Status Report" released by the International Energy Agency [2], carbon emissions from coal-fired power generation account for 30% of energy carbon emissions. Thus, developing an efficient method for CO_2 separation from flue gas is imperative.

The traditional method of removing CO_2 is to use alcohol amine solvent as absorbents, such as monoethanolamine (MEA) [3] and methyldiethanolamine (MDEA) [4]. But alcohol amine solvents are volatile and have poor stability, which can easily cause problems such as large solvent loss and high energy consumption [5]. In recent years, ionic liquids, with the unique properties of negligible vapor pressure, high chemical/thermal stability, good CO_2 solubility and fine adjustable capacity [6], have been widely used for the

* Corresponding authors.
E-mail addresses: cyang@fzu.edu.cn (C. Yang), tingqiu@fzu.edu.cn (T. Qiu).

https://doi.org/10.1016/j.gee.2020.12.019

separation of various CO_2 mixtures such as flue gas [7,8], natural gas [9] and syngas [10]. Blanchard et al. [11] first reported in 1999 that CO_2 is soluble in 1-butyl-3-methylimidazolium hexafluorophosphate [BMIM][PF_6], but IL is insoluble in CO_2, attracting wide attentions. Lei et al. [6] studied the solubility of various gases like CO_2, CO, N_2, SO_2 and O_2 in ILs and found that some ILs have high distinguishable solvation capacities for different gases. Pan et al. [12] designed several kinds of non-amino phosphonium ILs, which also showed excellent CO_2 absorption capacity. However, because of the numerous possible combinations of cations and anions in ILs which may be as high as 10^6 [13], experimental studies are time-consuming and expensive to measure properties of all ILs. Therefore, a priori screening simulation for designing favorable ILs is desirable.

Until now, several thermodynamic models have been applied for predicting properties of ILs, such as COSMO-RS [14,15], UNIFAC [16,17], equations of state (EoS) [18] and so forth. Among them, EoS which require temperature and pressure parameters have high accuracy, but they are limited by different systems and application range. The UNIFAC model based on group contribution method (GC) has higher accuracy than other models, since group interaction parameters in GC are fitted by a large amount of experimental data. The COSMO-RS model only needs the quantum-chemically derived surface charge density profiles (σ-profile) and cavity volumes (V_{COSMO}) of molecules without any experimental data. Although the prediction of the COSMO-RS model has a relatively bigger error, linear correction can improve its accuracy [13,19]. Regarding a large range of ILs, the COSMO-RS model is more suitable to be a priori model.

From a practical point of view, physical properties and process performance of ILs still need to be considered for using ILs in process production. The physical property limitations for a complete design standard are put forward including the melting point (T_m) and the viscosity (η) [16,20,21]. These two physical properties are usually estimated by various GC or quantitative structure–property relationship (QSPR) models [22–26]. For the viscosity of ILs, Lazzús et al. [27] developed the viscosity model based on 1445 experimental viscosity data of 326 ILs and GC, whose mean absolute percentage error (MAPE) is only 4.5%. Paduszyński and Domańska et al. [25] established a GC-based feed-forward artificial neural network (FFANN) model fitted by 13,000 experimental viscosity data of 1484 ILs, which gives mean square error of 0.0603 log units in the testing set. It has been found that these viscosity models have high accuracy and reliable prediction results.

For melting points of ILs, Lazzús et al. [23] proposed the model consisting of 400 ILs by GC and genetic algorithm, whose MAPE is 7.07%. Based on 667 experimental ILs data, Valderrama et al. [24] used back-propagation neural networks with GC to set up the model, whose mean absolute deviations of training and testing sets are 3.7% and 14.6%, respectively. Venkatraman et al. [28] applied various machine learning approaches with semi-empirical (PM6) electronic, thermodynamic and geometrical descriptors for prediction of melting points of 2212 ILs, which have only moderate accuracy of prediction. Among the models, the GC model built by Lazzús et al. [23] was usually applied for large-scale screening of ILs because of low MAPE and wide scope of applications [16,20,21]. Nevertheless, it should be pointed out the GC model of Lazzús et al. [23] consists of 400 ILs, which is not accurate enough to predict melting points of thousands of ILs. For instance, for the melting point of 1-octyl-3-methylimidazolium hexafluorophosphate [C_8MIM][PF_6], the prediction value is 339.104 K, which is much larger the experimental value (233.15 K). The large deviation of the melting point would significantly affect the results of large-scale screening of ILs. Therefore, a more accurate and applicable model is highly desirable. From the studies above, it is known that predicting the melting point of IL is not easy because of the complex structure of IL and unclear mechanisms [29]. Valderrama et al. [29] summarized some observed laws: (1) with the cationic chain length increasing, the melting temperature of IL first decreases, then increases and finally tends to be constant; (2) low symmetry, weak intermolecular interactions and a good distribution of charge in the cation may lead to low melting temperature. Therefore, it can be found that the melting point variation of IL is a nonlinear process and only using GC methods can not well describe these cases.

Nowadays, machine learning has been widely applied for the prediction of thermodynamic and physicochemical properties of ILs including solubility, density, viscosity, surface tension, heat capacity and so on [30–35]. Due to the ability to learn and handle complex problems efficiently, support vector machine, one of machine learning approaches, has been successfully used to estimate properties of ILs. For a large quantity set consisting of 22,268 data points of 2068 distinct ILs, Paduszyński et al. [26] built the viscosity model with R^2 of 0.9172 by least-squares support vector machine (LSSVM) and GC. Song et al. [34] established the SVM-GC model with high R^2 of 0.9783 for 10,116 CO_2 solubilities in ionic liquids. These cases showed that SVM with GC models can well deal with the nonlinear regression for estimation of melting points of IL.

In this work, in order to improve prediction accuracy and range of IL melting points, an SVM model is built. Then, for CO_2 separation from flue gas, optimal ILs are chosen based on COSMO-RS calculation and physical properties constraints. Finally, process performances and economic analysis of IL candidates and IL reported are evaluated by process simulations, so as to obtain the best IL.

2. Screening strategy

The screening strategy includes four steps: (1) determining the target system; (2) based on the corrected COSMO-RS model, calculating absorption, selectivity and desorption for each IL; (3) limiting physical properties of ILs to gain optimal ILs by viscosity model reported and melting points model

built in this work; (4) evaluating the process performances of optimal ILs and excellent IL reported in the literature by Aspen Plus. The screening strategy can be applied for many systems and CO_2 separation from flue gas is considered as the target system in this work. Schematic of the screening strategy is given in Fig. 1.

2.1. COSMO-RS model

The COSMO-RS model, a thermodynamic model for the prediction of some basic properties of the solvent, is first developed by Klamt and Eckert [36]. Nowadays, the COSMO-RS model has been widely used for priori screening of ILs without requiring any experimental data. The Henry's law constant is defined through Eq. (1):

$$H_i^s = \gamma_i^\infty P_i^s \tag{1}$$

where P_i^s is the saturated vapor pressure of compound i; γ_i^∞ is the infinite dilute activity coefficient of compound i in the solution s; H_i^s represents the Henry's law constant of compound i in solution s.

It can be found that the Henry's law constant above is calculated on a molar basis. Manesh et al. [37] and Dai et al. [38] pointed out that the solubility of CO_2 in IL will gradually increase with the molecular weight of IL growing. Thus, the mole-based method may be able to gain the ILs with very high molecular weight. It has been demonstrated that the CO_2 solubility in ILs with large molar weight is not high in mass or volume units compared to conventional organic solvents [39], which will cause more energy loss for the applications in the industry [40]. Since it is more desirable to select IL based on better mass-based performance, the calculation standards in this work are on a mass basis. The mass-based Henry's law constant is defined as follow:

$$H_i^{s'} = H_i^s \times \frac{M_{IL}}{M_i} \tag{2}$$

where M_{IL} and M_i represent the molecular weights of IL and gas compound i, respectively.

In addition to calculating the solubility of IL-containing systems, the selectivity toward different components in the gas mixture and the desorption capacity are also important for the performance of ILs. Farahipour et al. [19] defined the absorption−desorption index (ADI) to study solubility and desorption of CO_2 in ILs, and triethylsulfonium acetate [S_{222}][OAc] is selected to be the best IL. But selectivity of systems in actual process needs to be considered. Zhao et al. [13] established the absorption separation index (ASI), and studied ASI and ADI to gain optimized ILs methyl (diethyl)sulfonium tricyanomethanide [S_{221}][TCM] for CO_2/CH_4 separation and [S_{222}][OAc] for C_2H_2/C_2H_4 separation. However, they ignored the overall integration of absorption, selectivity and desorption. More recently, Wang et al. [20] combined the views of Farahipour et al. [19] and Zhao et al. [13], and proposed a mass-based Absorption-Selectivity-Desorption index (ASDI) integrating the gas solubility, selectivity, and desorption capacity of IL-containing systems which can well describe most thermodynamic properties of ILs. Based on ASDI, 3-(2-Carboxyethyl)-1-methylpyridinium acetate [$MPy_{13}(CH_2)_2COOH$][OAc] is selected to be the best solvent for CO_2 separation from flue gas. Thus, ASDI is the most comprehensive indicator and used in this work. Referring to a mass-based ASDI index, solvent selectivity and desorption capacity on a mass basis are determined in Eqs. (3) and (4):

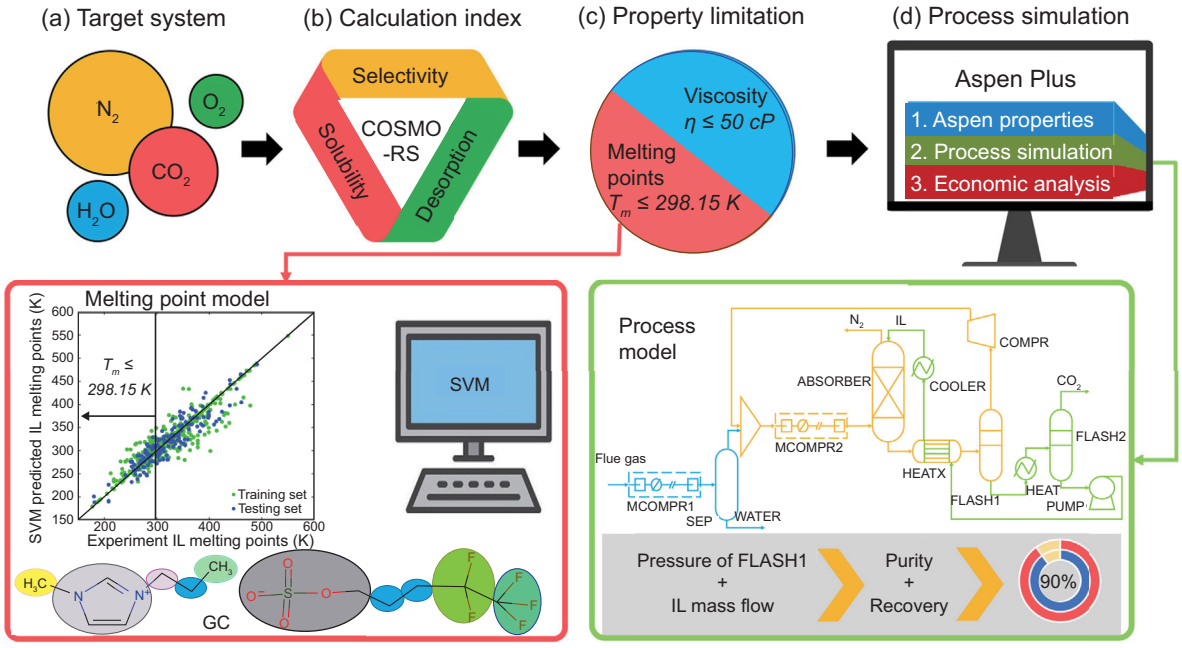

Fig. 1. Schematic of the screening strategy.

$$S_{i/j}=\frac{H_i^s}{H_j^s}\times\frac{M_j}{M_i} \tag{3}$$

$$D=\frac{H^{abs}}{H^{des}} \tag{4}$$

where H_j^s and M_j is the Henry's law constant of compound j in solution s and the molecular weight of compound j. $S_{i/j}$ is the mass-based selectivity. D is the mass-based desorption capacity of IL. H^{abs} and H^{des} represent the Henry's law constants at the assumed absorption and desorption temperatures, which are set at 298.15 K and 323.15 K, respectively.

As mentioned above, a mass-based Absorption-Selectivity-Desorption index, ASDI, is defined in Eq. (5):

$$ASDI=H_i^{s'}\times S_{i/j}\times D \tag{5}$$

From the definition of ASDI, it is known that smaller value of ASDI is, better IL capability for CO_2 separation is.

2.2. Physical property constraints

For applications in industrial production, the viscosity and melting point of ILs usually need to be limited. Thus, these physical property constraints proposed by Wang et al. [21] are given as follows:

$$T_m\le 298.15\ \mathrm{K} \tag{6}$$

$$\eta\le 50\ \mathrm{cP} \tag{7}$$

For the prediction of viscosity of ILs, a GC-based feed-forward artificial neural network model [25] that has been proved to be reliable [20] is used. For the prediction of melting points of ILs, an SVM model is built and used.

Support vector machine is a popular machine learning algorithm because it can map the input into a high-dimensional feature space and deal with many nonlinear or more complicated problems. The SVM model in the study is used by virtue of LIBSVM toolbox [41], which has many auxiliary functions that can help improve the performance of the model. The keys of the SVM model are the used kernel function, the corresponding kernel parameters and some internal parameters of the algorithm, which determine the performance of the model.

The prediction function of the SVM model is seen in Eq. (8):

$$f(x)=\sum_{i=1}^{l}\alpha_i K(x,x_i)+b \tag{8}$$

where x, x_i and $f(x)$ represent the input vector, i-th feature vector and the output respectively. α_i and b are the weights for this feature vector and bias. $K(x,x_i)$ is an used kernel function and the Gaussian radial basis function (RBF) kernel is selected in this work.

$$K(x,x_i)=exp\left(-gamma\cdot\|x-x_i\|^2\right) \tag{9}$$

where *gamma* is an adjustable parameter of the RBF function. By default, the kernel parameter *gamma* is equal to reciprocal of feature number.

2.3. Model correction

The COSMO-RS model has been proved to be a useful priori model without relying on any experimental data. However, the accuracy of the model usually only satisfies qualitative analysis because of the high deviation between experimental and COSMO-RS predicted physical properties. Thus, Zhao et al. [13], Farahipour et al. [19], Taheri et al. [42], and Liu et al. [43] developed the corrected COSMO-RS models with linear correction on the Henry's law constants and activity coefficients. These corrected models usually have better performances than the original COSMO-RS model. In this work, the correcting approach is used to improve the reliability of the COSMO-RS model, and COSMOthermX (version C3.0, release 18.01) is applied for predicting Henry's law constants of gases in ILs. The calculated results are compared with experimental data using the average absolute relative deviation (AARD) as follow:

$$AARD=\frac{100\,\%}{N}\sum_{i=1}^{N}\frac{\left|H_{i,exp}-H_{i,cal}\right|}{H_{i,exp}} \tag{10}$$

where N is the total number of data points. In this work, there are 463 experimental data points including two gases (CO_2 and N_2), obtained by Wang et al. [20].

Since the Henry constant values of the two gases vary significantly, the data points are plotted in $\log_{10}$ units, as seen in Fig. 2. Fig. 2a and b present a comparison between experimental and calculated values before and after correction, respectively. It can be seen that most of the calculated values have been adjusted to near the diagonal and are almost equal to the experimental values through correction. Corrected model is given in Eq. (11):

$$\log_{10}H_{cor}=1.1422\log_{10}H_{cal}-0.4664 \tag{11}$$

where H_{cal} is calculated Henry constant value by the COSMO-RS model and H_{cor} is corrected Henry constant value by Eq. (11). Note that R^2 of the model is 0.9383.

After correction, the AARD of whole data points reduces from 60.91% to 16.09%, which is similar to the deviation (15.63%) between experimental values and calculated values by Wang et al. [20]. That is to say, linear correction on the Henry's law constant is a reasonable method and the corrected model can meet the requirements of quantitative calculation.

2.4. Model validation

The SVM model is established on the basis of 768 experimental melting points data of 768 ILs, consisting of 29 cation groups and 39 anion groups as well as 31 substituents. The cations contain imidazolium, pyridinium, pyrrolidinium, piperidinium, oxazolidinium, guanidinium, morpholinium, isoquinolinium, sulfonium, ammonium, phosphonium and so forth; while the anions consist of borates, halides, sulfates and so on. Experimental melting points data of common ILs come from Venkatraman et al. [28] and have been preprocessed (see

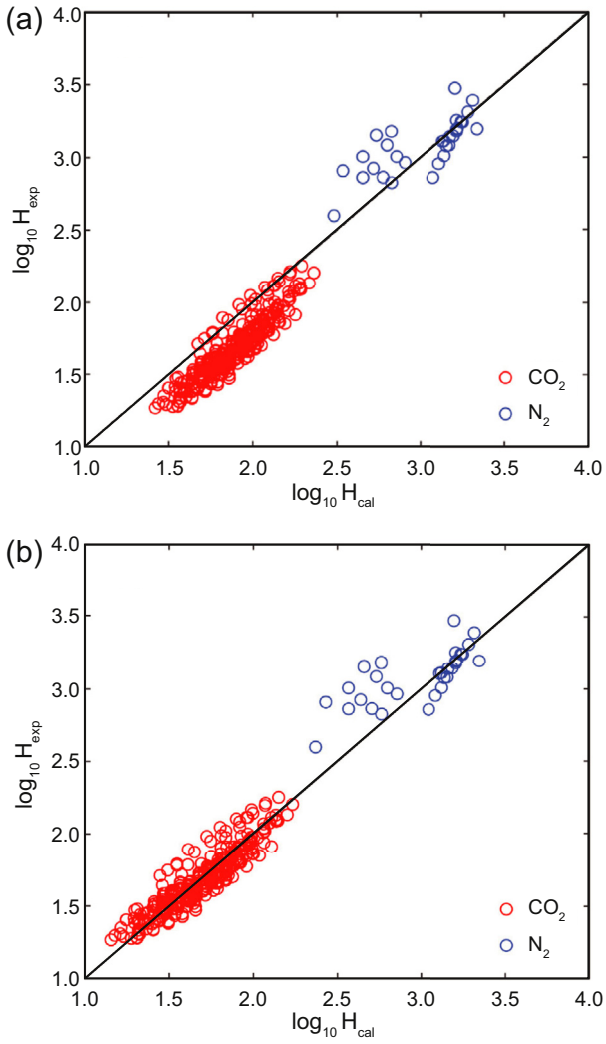

Fig. 2. Experimental $\log_{10}H_{exp}$ versus COSMO-RS calculated Henry's law constants $\log_{10}H_{cal}$ (a) before correction and (b) after correction.

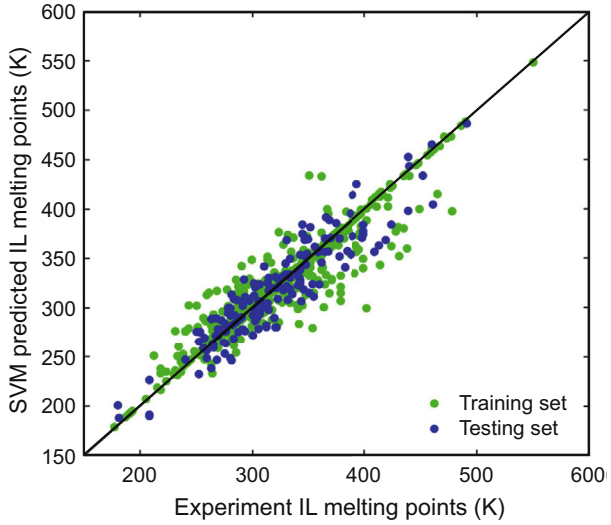

Fig. 3. Experimental $T_{m,exp}$ versus the SVM model predicted $T_{m,cal}$ in training set and testing set.

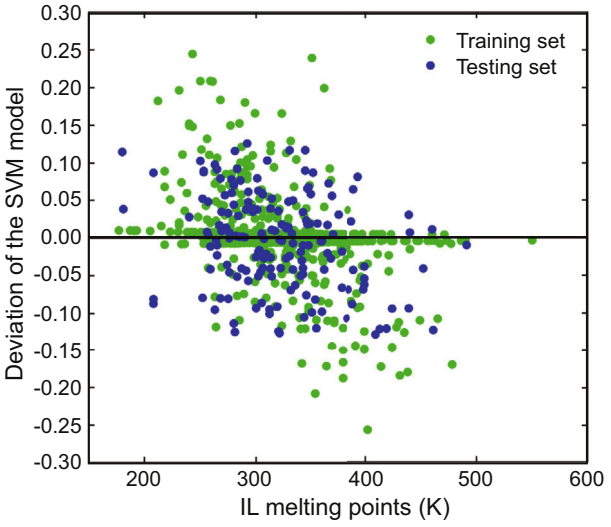

Fig. 4. The deviation of melting points of IL predicted by the SVM model.

the detailed data in Supporting Information Data1). Selecting 600 points from the data set are used as the training set and the rest points are used as the testing set. As the value of the melting point is much larger than the number of groups constituting the ionic liquids, melting points data and groups data need to be normalized. In order to get the best gamma value, the grid optimization method is used to find bestc and bestg, which are the best penalty parameter and gamma value, respectively. More model parameters are given in the SVM model of Supporting Information Data1.

Fig. 3 shows the comparison between experimental and SVM predicted melting points of ILs for training and testing data. It can be seen that most of the melting points data can be fitted well and only a few points have relatively larger errors. The residual plot is given in Fig. 4, which shows that the deviations of 99.09% data points are within 0.2 and 74.35% data points are below 0.05, indicating that the overall performance of the model is good. The estimated AARD and R^2 for the training set and the testing set are given in Table 1. It has been found that the performance of the testing set is not as good as the training set, but the testing set still has high accuracy. Table 2 shows several previous models for prediction of melting points of ILs. These models are based on diverse and numerous ILs. Although the previous models used various methods, such as GC, electronic descriptors, optimization algorithm and so forth, the combination of SVM + GC is first applied in the literature to be predicted melting points of ILs. It should also be noted that the GC method makes the model

Table 1
Statistical indicators of the SVM model.

Model	Training set		Testing set	
	AARD	R^2	AARD	R^2
SVM	3.11%	0.8820	5.12%	0.8542

Table 2
Review of previous model for prediction of melting points of ILs.

Authors	Model	Ionic liquids	Regression	Results
Lazzús et al. [23]	GC	400 Diverse	Genetic algorithm	R^2 = 0.8841, AARD = 7.07%,
Gharagheizi et al. [22]	GC	799 Diverse	Optimization algorithm	598 ILs: $R^2_{training}$ = 0.81, 201 ILs: $R^2_{testing}$ = 0.82, AARD = 5.82%
Farahani et al. [44]	Constitutional, 2D and 3D	705 Diverse	Genetic function approximation	563 ILs: $R^2_{training}$ = 0.66, 142 ILs: $R^2_{testing}$ = 0.72, AARD = 7.30%
Valderrama et al. [24]	GC	667 Diverse	Back-propagation neural networks	567 ILs: $AARD_{training}$ = 3.70%, 100 ILs: $AARD_{testing}$ = 14.60%
Venkatraman et al. [28]	electronic, thermodynamic and geometrical descriptors	2212 Diverse	Various machine learning approaches	Cubist, 1486 ILs: $R^2_{training}$ = 0.67, 726 ILs: $R^2_{testing}$ = 0.64

only need structure information and the SVM regression method helps the model predict melting points of ILs with complex structures. Comparing with other models, the SVM model which has lowest AARD based on the moderate number of ILs is applied to melting points prediction of ILs in the study.

2.5. Results and discussion

2.5.1. Ionic liquids selection

In order to gain optimized IL for CO_2 separation from flue gas, the corrected COSMO-RS model is applied for predicting Henry's law constants of each IL. Based on the reported solvents in the literature, the cations and anions involved in this work include imidazole, pyridine, pyrrolidine, hexafluorophosphate, tetrafluoroborate, bis(trifluoromethylsulfonyl)imide, and so on. More ions and Henry's law constants calculated by the corrected COSMO-RS model for each combination of anions and cations are shown in Supporting Information Data1.

2.5.2. Screening results

Based on the aforementioned thermodynamic and physical models, the mass-based ASDI index arranged from small to large is calculated. Then, for meeting the physical properties constraints, the best five ILs with the smallest ASDI values can be obtained in Table 3. From a cation point of view, cations of these five ILs are all pyrrolidines including 1-ethyl-1-methylpyrrolidinium $[EMPYR]^+$ and 1-methyl-1-propylpyrrolidinium $[C_3C_1PYR]^+$. Zhao et al. [13] indicated that ILs with pyrrolidines cations have lower viscosity. Focusing on more important anions, it is found that anions of the best five ILs are cyanide anion. Carvalho et al. [39], Palomar et al. [40], Mota et al. [45] and Gupta et al. [46] showed that cyano-based ILs have high solubility and selectivity in physical absorption of CO_2. For the whole five ILs, they have the characteristics of low molecular weight and low viscosity which are also proved to be key parameters to minimize solvent consumption, energy duty and equipment size by Palomar et al. [40]. It is believed that the selected five ILs in this work have great potential for CO_2 separation from flue gas. Compared with IL $[MPy_{13}(CH_2)_2COOH][OAc]$ reported by Wang et al. [20], optimized five ILs have significant advantages in mass-based ASDI and selectivity as well as viscosity, but they are not good enough in mass-based Henry's constant and desorption. As seen in Table 3, the mass-based selectivity, mass-based ASDI and viscosity of $[MPy_{13}(CH_2)_2COOH][OAc]$ are 3.96, 2.46 and 2.34 times larger than that of designed IL $[C_3C_1PYR][TCB]$, respectively. It is interesting to note that the melting points model used in Wang et al. [20] is the GC model established by Lazzús et al. [23]. For the anion $[TCB]^-$, the estimation of the GC model has a large error, such as [EMIM][TCB] (predicted value is 565.67 K, experimental value is 281.45 K and deviation is 100.98%) and 1-butyl-1-methylpyrrolidinium tetracyanoborate $[C_4C_1PYR][TCB]$ (predicted value is 592.03 K, experimental value is 293.15 K and deviation is 101.96%). When the two ILs are estimated by the SVM model in this work, predicted values of [EMIM][TCB] and $[C_4C_1PYR][TCB]$ are 279.59 K and 295.05 K, respectively. Moreover, the predicted deviations of two ILs are about 0.65%. Thus, a more accurate model of ILs is beneficial to the wide selection of ILs.

3. Process evaluation

To further assess the abilities of ILs, process performances of optimal ILs are evaluated by process simulation. Recently,

Table 3
Optimized ILs with their properties in comparison with IL reported in the literature for the CO_2/N_2 separation.

No.	ILs	*MW*	*H′* (bar)	*S′*	*D′*	*ASDI* (bar)	T_m (K)	η (cP)
1	$[C_3C_1PYR][TCB]$	243.12	76.32	0.0091	0.520	0.362	296.59	41.09
2	[EMPYR][DCA]	180.25	87.13	0.0104	0.509	0.460	242.56	24.29
3	[EMPYR][TCM]	204.27	95.39	0.0102	0.526	0.514	271.26	26.03
4	$[C_3C_1PYR][TCM]$	218.30	92.78	0.0107	0.529	0.525	269.60	32.33
5	$[C_3C_1PYR][DCA]$	194.28	94.19	0.0107	0.523	0.525	240.00	32.91
Ref.	$[MPy_{13}(CH_2)_2COOH][OAc]$	224	60.11	0.036	0.41	0.89	268.38	96.30

Song et al. [47] introduced ILs into Aspen Plus to study their properties and test their performances. ILs are used as user-defined components or pseudo-components in Aspen Plus by specifying their molecular weights, densities, normal boiling points, critical properties, and so on [48]. Subsequently, the corresponding physical method is used to simulate industrial processes, which has been demonstrated to be reliable for the process simulation of ILs [49,50].

3.1. Computation details

In this work, Aspen Plus V 9.0 is applied for process simulation and the COSMO-SAC model is used as the physical method. The molecular weight is given by COSMOthermX. The normal boiling point is estimated by Valderrama et al. [51]. The density, heat capacity, viscosity, surface tension and thermal conductivity of the ILs are specified using physical property equations in Aspen Plus with regressed parameters from experimental data. For each component, the molecular volumes (CSACVL) and the σ-profiles parameters (SGPRF1 to SGPRF5) from corresponding cosmo files calculated by TurbomoleX 7.4 specify the original COSMO-SAC property model. Because of the dominant role of anions [52–54] and ILs candidates without experimental data [EMIM][TCB], [EMIM][TCM] and [EMIM][DCA] are selected to simulate process compared with [EMIM][Tf_2N] reported by Riva et al. [55], which has low viscosity, high absorption capacity and low molecular weight.

3.2. Physical properties verification

The fuel gas consists of CO_2 (13.4 mol%), N_2 (74.2 mol%), O_2 (5.0 mol%), and H_2O (7.4 mol%) [55]. H_2O in flue gas is first removed because its high heat capacity will cause high energy consumption. N_2 and O_2 in flue gas have very low solubility in ILs [52,56]. Thus, vapor–liquid equilibrium values of binary IL–CO_2 systems are estimated to validate COSMO-based Aspen Plus calculations. Fig. 5a, b, c and d present vapor–liquid equilibrium data of binary IL [EMIM][TCB], [EMIM][TCM], [EMIM][DCA] and [EMIM][Tf_2N] with CO_2 systems, respectively. It can be seen that the results of [EMIM][TCB], [EMIM][TCM], and [EMIM][Tf_2N] are highly consistent with experimental values, since their AARDs are 9.48%, 6.26% and 6.09%, respectively. But it should be noted that the solubility of [EMIM][DCA] with AARD of 63.19% is overestimated by Aspen Plus. Palomar et al. [40] also reported the same situation that solubility of CO_2 in [EMIM][DCA] predicted by the same COSMO-SAC model in Aspen Plus is about twice the experimental values. In addition, [EMIM][DCA] lacks more experimental solubility data and can't be further verified. Thus [EMIM][DCA] will not be used in the next process.

Properties of ILs including [EMIM][TCB], [EMIM][TCM] and [EMIM][Tf_2N] are given in Table 4. The Andrade parameters of [EMIM][TCM] and [EMIM][Tf_2N] are from Riva et al. [57] and parameters of [EMIM][TCB] are fitted by

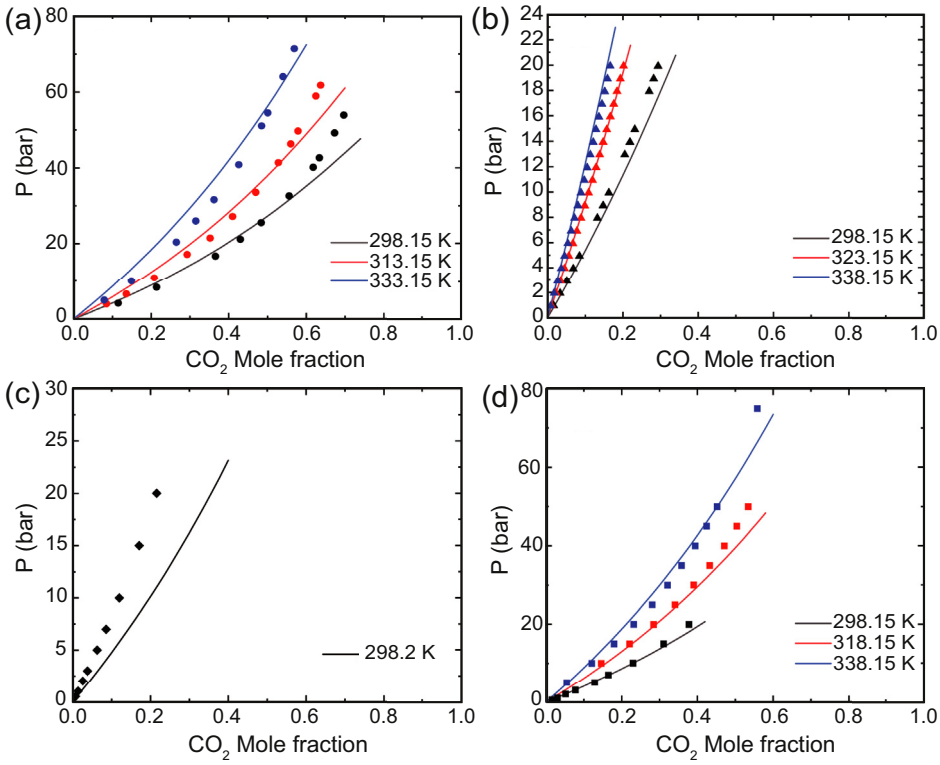

Fig. 5. Vapor-liquid equilibrium data of binary IL–CO_2 systems: (a) [EMIM][TCB], (b) [EMIM][TCM], (c) [EMIM][DCA], (d) [EMIM][Tf_2N]. Points: experimental data and solid lines: prediction by Aspen Plus.

Table 4
Properties of [EMIM][TCB], [EMIM][TCM] and [EMIM][Tf_2N] defined in Aspen Plus.

Property	[EMIM][TCB]	[EMIM][TCM]	[EMIM][Tf_2N]
Molecular weight (MW), (g mol^{-1})	226.047[a]	201.229[a]	391.31[a]
Boiling point (TB), (K)	952.22[b]	869.37[b]	816.70[b]
COSMO volume (CSACVL), ($Å^3$)	302.77[a]	267.85[a]	357.48[a]
Viscosity parameter (MULAND)	−120.829[a]	−5.5104[c]	-6[c]
	8164.58[a]	2432.1[c]	2826.4[c]
	16.911[a]		

[a] This work.
[b] Ref. (Valderrama et al., 2015 [50]).
[c] Ref. (Riva et al., 2014 [57]).

experimental data in this work. More IL properties and verification are shown in Supporting Information Data2.

3.3. CO_2 absorption process design

The process flow sheets based on Ma et al. [58] are shown in Fig. 6, including flue gas drying (the blue area), CO_2 absorption (the orange area) and IL regeneration (the green area), to compare the performance of each IL. The flue gas drying consists of the multistage compressor (MCOMPR1) and the gas–liquid separation tank (SEP). The flue gas is first compressed and cooled in MCOMPR1, and removes much water in SEP. Subsequently, for CO_2 absorption, dehydrated flue gas is recompressed in the multistage compressor (MCOMPR2) and fed to the absorption tower (ABSORBER) where the gas comes into countercurrent contact with the IL entering the top of the tower and is absorbed. The IL coming out of the bottom of ABSORBER is heated in the heat exchanger (HEATX) and transferred to a flash tower (FLASH1). Then, N_2 and a small amount of CO_2 are desorbed in the top of FLASH1, compressed in the compressor (COMPR), and returned to ABSORBER. For IL regeneration, the IL in the bottom of FLASH1 is heated in the heater (HEAT) and desorbed in the flash tower (FLASH2) to regenerate the IL and gain pure CO_2. The regenerated IL is compressed by the pump (PUMP), cooled by HEATX, and finally returned back to ABSORBER.

Since the number of the theoretical stage is important for the design of the absorption tower, the sensitivity analysis of the stage is given in Fig. 7. Moreover, the CO_2 removal rate in the absorption tower is used to evaluate the sensitivity analysis performance and defined in Eq. (12), following Liu et al. [10]. Fig. 7 shows the IL mass flow required of different stages for each IL when the CO_2 removal rate reaches 95%. It is found that the decrease of IL mass flow is significant when the theoretical stage increases from 15 to 20. Nevertheless, the further increase of the theoretical stage results in slight decrease of IL mass flow. With the considerations of the equipment cost and operating cost, it is believed that 20 stages are the most suitable for this process, which is consistent with Shiflett et al. [59]. Thus, the absorption tower is modeled with 20 theoretical stages and 23.2 m packing height based on the rate-based model. The pressure of the absorption tower is set to 30 bar, the diameter of which is calculated to preserve a fractional capacity of 80% in all the processes. The Flexiring random (0.016 m) is used to capture CO_2. The flow rate of flue gas is 100 kmol h^{-1} at 50 °C and 1 bar. The process parameters of IL-based systems are given in Table 5. The performances of the three ILs are evaluated with roughly equal recovery and purity of CO_2, defined in Eqs. (13) and (14):

$$CO_{2,removal} = 1 - \frac{mole\ flow\ of\ CO_2\ in\ gasout\ stream\ top\ in\ ABSORBER}{CO_2\ mole\ flow\ in\ flue\ gas} \quad (12)$$

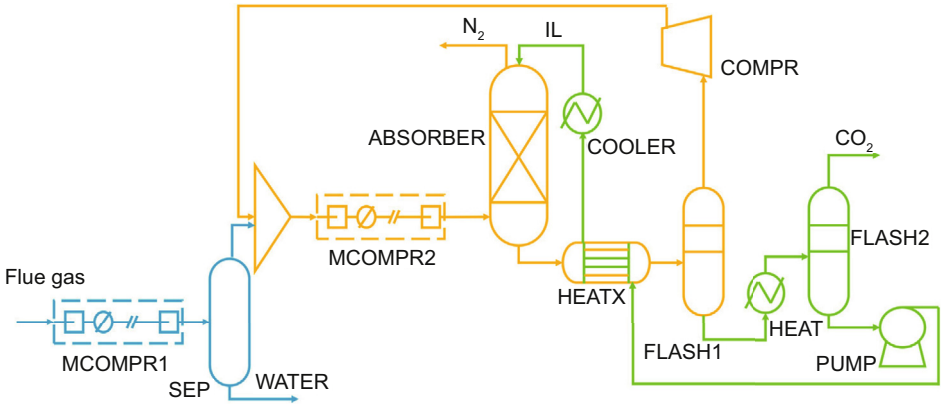

Fig. 6. The process flow sheet.

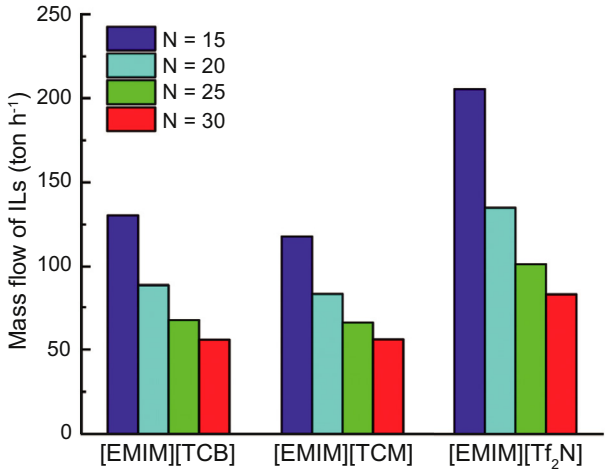

Fig. 7. Sensitivity analysis of stages for three ILs [EMIM][TCB], [EMIM][TCM] and [EMIM][Tf_2N]. N is stage number.

$$CO_{2,recovery} = \frac{CO_2\ mole\ flow\ in\ gasout\ stream\ top\ in\ FLASH2}{CO_2\ mole\ flow\ in\ flue\ gas} \tag{13}$$

$$CO_{2,purity} = \frac{CO_2\ mole\ flow\ in\ gasout\ stream\ top\ in\ FLASH2}{mole\ flow\ in\ gasout\ stream\ top\ in\ FLASH2} \tag{14}$$

The key conditions ensuring consistent recovery and purity of CO_2 in each process are the mass flow of IL and the pressure of FLASH1 when the pressure of FLASH2 is fixed. Fig. 8 shows the variation of CO_2 recovery and purity, as the IL flow rate and FLASH1 pressure change, respectively. It can be seen that with the increase of mass flow of IL, the recovery of CO_2 arises, but the purity of CO_2 drops. The interpretation is that the increased mass flow rate of IL will absorb more CO_2 and N_2. Similarly, increasing the FLASH1 pressure will cause the flow rates of CO_2 and N_2 to rise in the IL at the bottom of FLASH1. Thus, adjusting these two parameters can get the best operating conditions. As shown in Fig. 8, the mass flow of ILs and the pressure of FLASH1 are set 81 ton h^{-1} and 5.5 bar for [EMIM][TCB], 77 ton h^{-1} and 6.4 bar for [EMIM][TCM], and 152 ton h^{-1} and 3.7 bar for [EMIM][Tf_2N].

3.4. Cost estimation methodology

In this work, the total annualized cost (TAC) is calculated to evaluate the performance of each IL. TAC is the sum of the annualized capital cost (ACC) and annualized operating expense (OPEX). ACC is converted from the total capital expense (CAPEX) by calculating the annual interest rate as follow:

$$ACC = OPEX \times \frac{r(1+r)^n}{(1+r)^n - 1} \tag{15}$$

where r and n refer to annual interest rate and the lifetime of the project, which are set to 8% and 25 years in this work, respectively [7].

CAPEX mainly includes direct cost (DC), indirect cost (IC), working capital and solvent cost, as seen in Table S3 in Supporting Information Data2, following Liu et al. [10]. A method based on the percentage of purchased equipment cost (PEC) is used to estimate the total capital costs [9]. PEC of each process is estimated by the software Aspen process economic analyzer (APEA). Based on the estimation of Riva et al. [55], prices of ILs are set to be 50 \$ kg^{-1} in the future with production on a large scale. OPEX consists of variable costs (VC) and fixed costs (FC). Solvent make-up is included in VC and annualized IL make-up is calculated based on 0.35 g ton^{-1} CO_2 [60] because of the non-volatile characteristics of IL.

3.5. Results of process evaluation

The results of the process evaluation for each IL are given in Table 6. When gaining the same CO_2 recovery of each IL, relevant flow data like the flow rate of IL are identified. It can be seen that the mass flow rates of selected ILs are almost half of that of IL reported. From the perspective of economic analysis, the processes of cyano-based ILs have lower ACC and TAC than that of [EMIM][Tf_2N]. The interpretation is that the cyano-based ILs have smaller molecular weight and viscosity as well as higher CO_2 solubility. Finally [EMIM][TCM] is selected to be the best IL and its process leads to 12.9% savings on TAC compared to that of [EMIM][Tf_2N], which proves the result of the screening strategy.

Table 5
Process parameters of IL-based systems.

Specification	[EMIM][TCB]	[EMIM][TCM]	[EMIM][Tf_2N]
ABSORBER			
Feed temperature (K)	298.15	298.15	298.15
Top pressure (bar)	30	30	30
Number of theoretical stages	20	20	20
Column diameter (m)	0.96	0.96	0.88
FLASH1			
Temperature (K)	313.15	313.15	313.15
Pressure (bar)	5.5	6.4	3.7
FLASH2			
Temperature (K)	323.15	323.15	323.15
Pressure (bar)	0.01	0.01	0.01

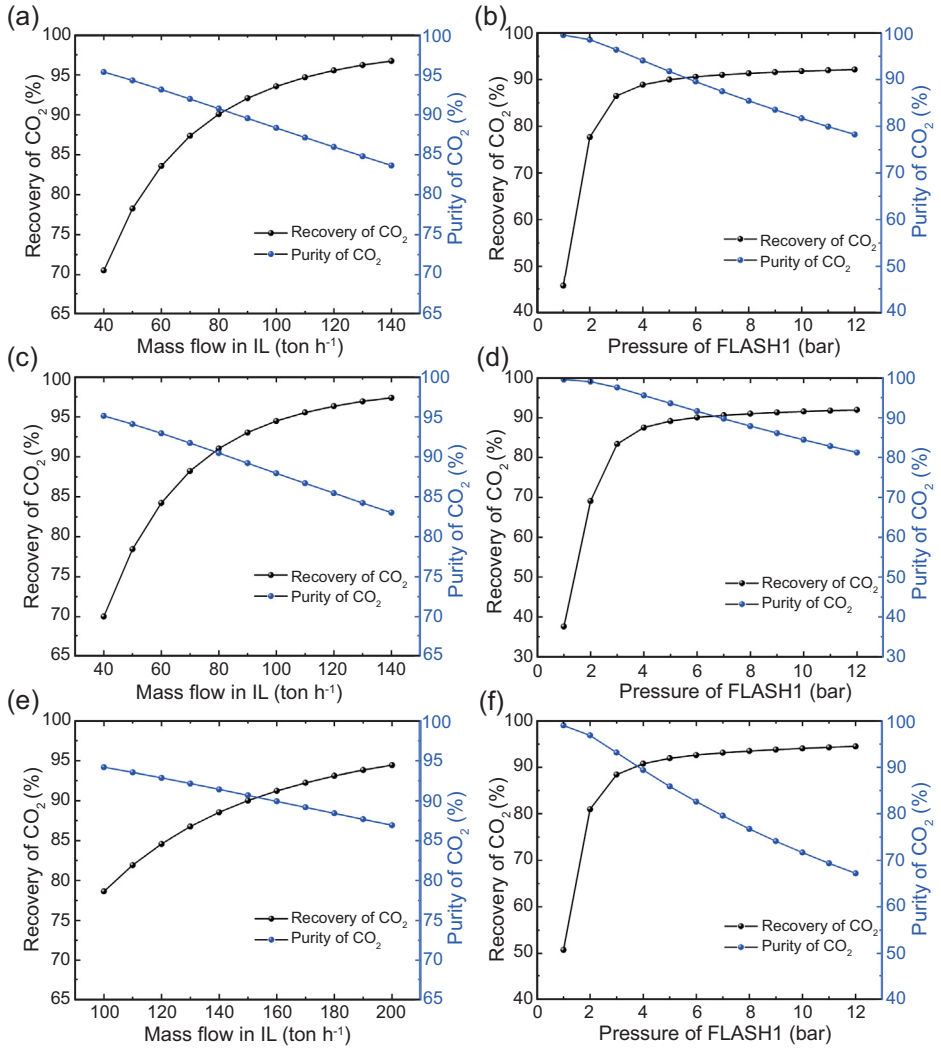

Fig. 8. Recovery and purity of CO_2 vary with mass flow of IL and pressure of FLASH1, respectively. (a)–(b) [EMIM][TCB], (c)–(d) [EMIM][TCM] and (e)–(f) [EMIM][Tf_2N].

Table 6
Results obtained from the process evaluation for each IL.

	[EMIM][TCB]	[EMIM][TCM]	[EMIM][Tf_2N]
IL mass flow (ton h^{-1})	81	77	152
CO_2 recovered from last flash (CO_2 stream) (kg h^{-1})	532.52	532.39	532.39
CO_2 recovery rate (%)	90.30	90.28	90.28
CO_2 purity in CO_2 stream (%)	90.65	90.84	90.52
CAPEX (M$)	15.12	14.87	18.88
ACC (M$)	1.42	1.39	1.77
OPEX (M$)	1.64	1.63	1.71
TAC (M$)	3.06	3.03	3.48

4. Conclusions

This work established a new model based on SVM and GC for predicting the melting points of ionic liquids. The SVM model covering 29 cation groups and 39 anion groups as well as 31 substituents consists of 768 experimental data and is validated to be reliable. Based on a systematic study, including evaluation of the absorption, selectivity and desorption of IL and constraints for its viscosity and melting points, cyano-based ILs were found to be excellent solvents for separating CO_2/N_2 gas mixture, in which anion $[TCB]^-$ was usually ruled out by incorrect estimation of the model with small IL range.

Finally, through the process simulation by Aspen Plus [EMIM][TCM] was selected as best IL, the process of which led to 12.9% savings on TAC compared to that of [EMIM][Tf_2N].

The SVM model is flexible to predict melting points of various ionic liquids with complex structures. However, it has a lot of difficulties, such as lacking of enough experimental data, unexplainable mechanisms, and so on. In future work, it is vital to study the mechanisms of melting points of IL for higher model accuracy and larger IL range. Furthermore, through the melting points model with a large IL range, it is probable to discover many new ionic liquids with great potential. These new ILs usually need to be synthesized and measured for physical properties before they can be put into use. Due to the length limitation of the article, these contents were not included in this work. Finally, these ILs can be evaluated by process simulation and applied to the development of ionic liquids industrialization.

Conflict of interest

The authors declare that they have no known competing financial interests or personal relationships that could have appeared to influence the work reported in this paper.

Acknowledgment

The authors wish to acknowledge the financial support by the National Natural Science Foundation of China (Project No. 21878054), the Natural Science Foundation of Fujian Province of China (2020J01515).

Appendix A. Supplementary data

Supplementary data to this article can be found online at https://doi.org/10.1016/j.gee.2020.12.019.

Nomenclature

σ	charge density, e $Å^{-1}$
V_{COSMO}	cavity volume, m^3
T_m	melting point, K
η	viscosity, cP
H_i^s	Henry's law constant of compound i in solution s, Pa
γ_i^∞	infinite dilute activity coefficient of compound i in the solution s
P_i^s	saturated vapor pressure of compound i, Pa
M	molecular weight, g mol^{-1}
$S_{i/j}$	mass-based selectivity
D	mass-based desorption capacity
H^{abs}	Henry's law constants at the assumed absorption temperature, Pa
H^{des}	Henry's law constants at the assumed desorption temperature, Pa
$ASDI$	mass-based Absorption-Selectivity-Desorption index, bar
$f(x)$	input vector
α_i	weights for feature vector
b	bias
$K(x, x_i)$	kernel function
N	stage number
r	annual interest rate

Abbreviations

ILs	ionic liquids
SVM	support vector machine
AARD	average absolute relative deviation
R^2	squared correlation coefficient
COSMO-RS	conductor-like screening model for real solvents
MEA	monoethanolamine
MDEA	methyldiethanolamine
UNIFAC	universal quasichemical functional−group activity coefficients
EoS	equations of state
GC	group contribution method
QSPR	quantitative structure−property relationship;
MAPE	mean absolute percentage error
COSMO-SAC	conductor-like screening model for segment activity coefficient
TAC	the total annualized cost
ACC	the annualized capital cost
OPEX	operating expense
CAPEX	capital expense
DC	direct cost
IC	indirect cost
PEC	purchased equipment cost
APEA	Aspen process economic analyzer
VC	variable charge
FC	fixed charge
[EMIM]	1-ethyl-3-methylimidazolium
[BMIM]	1-butyl-3-methylimidazolium
[C_8MIM]	1-octyl-3-methylimidazolium
[S_{221}]	methyl(diethyl)sulfonium
[S_{222}]	triethylsulfonium
[$MPy_{13}(CH_2)_2COOH$]	3-(2-Carboxyethyl)-1-methylpyridinium
[EMPYR]	1-ethyl-1-methylpyrrolidinium
[C_3C_1PYR]	1-propyl-1-methylpyrrolidinium
[C_4C_1PYR]	1-butyl-1-methylpyrrolidinium
[TCB]	tetracyanoborate
[TCM]	tricyanomethanide
[Tf_2N]	bis(trifluoromethylsulfonyl)amide
[PF_6]	hexafluorophosphate
[OAc]	acetate
[DCA]	dicyanamide

References

[1] WMO, Greenh Gas B. https://library.wmo.int/index.php?lvl=notice_display&id=3030#.X-ruMXbgJFA.
[2] IEA, Global Energy & CO_2 Status Report 2019. https://www.iea.org/reports/global-energy-co2-status-report-2019.
[3] T. Wang, J. Hovland, K.J. Jens, J. Environ. Sci.-China. 27 (2015) 276–289.
[4] M. Wang, A. Lawal, P. Stephenson, J. Sidders, C. Ramshaw, Chem. Eng. Res. Des. 89 (2011) 1609–1624.
[5] C.-H. Yu, C.-H. Huang, C.-S. Tan, Aerosol Air Qual. Res. 12 (2012) 745–769.
[6] Z. Lei, C. Dai, B. Chen, Chem. Rev. 114 (2014) 1289–1326.
[7] Y. Huang, X. Zhang, X. Zhang, H. Dong, S. Zhang, Ind. Eng. Chem. Res. 53 (2014) 11805–11817.
[8] L. Jiang, K. Mei, K. Chen, R. Dao, H. Li, C. Wang, Green Energy Environ. (2020), https://doi.org/10.1016/j.gee.2020.08.008.
[9] P. García-Gutiérrez, J. Jacquemin, C. Mccrellis, I. Dimitriou, S.F.R. Taylor, C. Hardacre, R.W.K. Allen, Energy Fuel. 30 (2016) 5052–5064.
[10] X. Liu, Y. Chen, S. Zeng, X. Zhang, S. Zhang, X. Liang, R. Gani, G.M. Kontogeorgis, AIChE J. 66 (2019) e16794.
[11] L.A. Blanchard, D. Hancu, E.J. Beckman, J.F. Brennecke, Nature 399 (1999) 28–29.
[12] M. Pan, N. Cao, W. Lin, X. Luo, K. Chen, S. Che, H. Li, C. Wang, ChemSusChem 9 (2016) 2351–2357.
[13] Y. Zhao, R. Gani, R.M. Afzal, X. Zhang, S. Zhang, AIChE J. 63 (2017) 1353–1367.
[14] C. Zhang, J. Wu, R. Wang, E. Ma, L. Wu, J. Bai, J. Wang, Green Energy Environ. (2020), https://doi.org/10.1016/j.gee.2020.08.001.
[15] J. Han, C. Dai, G. Yu, Z. Lei, Green Energy Environ. 3 (2018) 247–265.
[16] Z. Song, C. Zhang, Z. Qi, T. Zhou, K. Sundmacher, AIChE J. 64 (2018) 1013–1025.
[17] M. Mu, J. Cheng, C. Dai, N. Liu, Z. Lei, Y. Ding, J. Lu, Green Energy Environ. 4 (2019) 190–197.
[18] M.T.M. Martinez, M.C. Kroon, C.J. Peters, J. Supercrit. Fluids 101 (2015) 54–62.
[19] R. Farahipour, A. Mehrkesh, A.T. Karunanithi, Chem. Eng. Sci. 145 (2016) 126–132.
[20] J. Wang, Z. Song, H. Cheng, L. Chen, L. Deng, Z. Qi, ACS Sustain. Chem. Eng. 6 (2018) 12025–12035.
[21] J. Wang, Z. Song, X. Li, H. Cheng, L. Chen, Z. Qi, Ind. Eng. Chem. Res. 59 (2020) 2093–2103.
[22] F. Gharagheizi, P. Ilani-Kashkouli, A.H. Mohammadi, Fluid Phase Equil. 329 (2012) 1–7.
[23] J.A. Lazzús, Fluid Phase Equil. 313 (2012) 1–6.
[24] J.O. Valderrama, C.A. Faúndez, V.J. Vicencio, Ind. Eng. Chem. Res. 53 (2014) 10504–10511.
[25] K. Paduszyński, U. Domanska, J. Chem. Inf. Model. 54 (2014) 1311–1324.
[26] K. Paduszyński, Ind. Eng. Chem. Res. 58 (2019) 17049–17066.
[27] J.A. Lazzús, G. Pulgar-Villarroel, J. Mol. Liq. 209 (2015) 161–168.
[28] V. Venkatraman, S. Evjen, H.K. Knuutila, A. Fiksdahl, B.K. Alsberg, J. Mol. Liq. 264 (2018) 318–326.
[29] J.O. Valderrama, Ind. Eng. Chem. Res. 53 (2013) 1004–1014.
[30] A. Barati-Harooni, A. Najafi-Marghmaleki, A.H. Mohammadi, J. Mol. Liq. 231 (2017) 462–473.
[31] J.A. Lazzús, F. Cuturrufo, G. Pulgar-Villarroel, I. Salfate, P. Vega, Ind. Eng. Chem. Res. 56 (2017) 6869–6886.
[32] Y. Zhao, X. Zhang, L. Deng, S. Zhang, Comput. Chem. Eng. 92 (2016) 37–42.
[33] A. Barati-Harooni, A. Najafi-Marghmaleki, A.H. Mohammadi, J. Mol. Liq. 227 (2017) 324–332.
[34] Z. Song, H. Shi, X. Zhang, T. Zhou, Chem. Eng. Sci. 223 (2020) 115752.
[35] Y. Cao, J. Yu, H. Song, X. Wang, S. Yao, J. Serb. Chem. Soc. 78 (2013) 653–667.
[36] A. Klamt, F. Eckert, Fluid Phase Equil. 172 (2000) 43–72.
[37] S. Mortazavi-Manesh, M. Satyro, R.A. Marriott, Fluid Phase Equil. 307 (2011) 208–215.
[38] C. Dai, Z. Lei, B. Chen, AIChE J. 63 (2017) 1792–1798.
[39] P.J. Carvalho, K.A. Kurnia, J.A. Coutinho, Phys. Chem. Chem. Phys. 18 (2016) 14757–14771.
[40] J. Palomar, M. Larriba, J. Lemus, D. Moreno, R. Santiago, C. Moya, J. de Riva, G. Pedrosa, Separ. Purif. Technol. 213 (2019) 578–586.
[41] C.-C. Chang, C.-J. Lin, ACM T. Intel. Syst. Tec. 2 (2011) 1–27.
[42] M. Taheri, R. Zhu, G. Yu, Z. Lei, Chem. Eng. Sci. 230 (2021) 116199.
[43] X. Liu, T. Zhou, X. Zhang, S. Zhang, X. Liang, R. Gani, G.M. Kontogeorgis, Chem. Eng. Sci. 192 (2018) 816–828.
[44] N. Farahani, F. Gharagheizi, S.A. Mirkhani, K. Tumba, Thermochim. Acta 549 (2012) 17–34.
[45] M.T. Mota-Martinez, P. Brandl, J.P. Hallett, N. Mac Dowell, Mol. Syst. Des. Eng. 3 (2018) 560–571.
[46] K.M. Gupta, Fluid Phase Equil. 415 (2016) 34–41.
[47] Z. Song, X. Li, H. Chao, F. Mo, T. Zhou, H. Cheng, L. Chen, Z. Qi, Green Energy Environ. 4 (2019) 154–165.
[48] V.R. Ferro, C. Moya, D. Moreno, R. Santiago, J. de Riva, G. Pedrosa, M. Larriba, I. Diaz, J. Palomar, Ind. Eng. Chem. Res. 57 (2018) 980–989.
[49] D. Hospital-Benito, J. Lemus, C. Moya, R. Santiago, J. Palomar, Chem. Eng. J. 390 (2020) 124509.
[50] G. Yu, C. Dai, B. Wu, N. Liu, B. Chen, R. Xu, Green Energy Environ. (2020), https://doi.org/10.1016/j.gee.2020.10.022.
[51] J.O. Valderrama, L.A. Forero, R.E. Rojas, Ind. Eng. Chem. Res. 54 (2015) 3480–3487.
[52] M. Ramdin, T.W. de Loos, T.J.H. Vlugt, Ind. Eng. Chem. Res. 51 (2012) 8149–8177.
[53] S.N.V.K. Aki, B.R. Mellein, E.M. Saurer, J.F. Brennecke, J. Phys. Chem. B 108 (2004) 20355–20365.
[54] J.L. Anthony, J.L. Anderson, E.J. Maginn, J.F. Brennecke, J. Phys. Chem. B 109 (2005) 6366–6374.
[55] J. de Riva, J. Suarez-Reyes, D. Moreno, I. Díaz, V. Ferro, J. Palomar, Int. J. Greenh. Gas Con. 61 (2017) 61–70.
[56] G. Yu, X. Sui, Z. Lei, C. Dai, B. Chen, AIChE J. 65 (2019) 479–482.
[57] J. de Riva, V.R. Ferro, L. del Olmo, E. Ruiz, R. Lopez, J. Palomar, Ind. Eng. Chem. Res. 53 (2014) 10475–10484.
[58] Y. Ma, J. Gao, Y. Wang, J. Hu, P. Cui, Int. J. Greenh. Gas Con. 75 (2018) 134–139.
[59] M.B. Shiflett, D.W. Drew, R.A. Cantini, A. Yokozeki, Energy Fuel. 24 (2010) 5781–5789.
[60] T. Ma, J. Wang, Z. Du, A.A. Abdeltawab, A.M. Al-Enizi, X. Chen, G. Yu, Int. J. Greenh. Gas Con. 58 (2017) 223–231.